PCCP

RSC Publishing

PAPER

Keggin heteropolyacid $H_3PW_{12}O_{40}$ supported on different oxides for catalytic and catalytic photo-assisted propene hydration†

Cite this: *Phys. Chem. Chem. Phys.*, 2013, **15**, 13329

G. Marcì,*[ab] E. García-López,[ab] M. Bellardita,[ab] F. Parisi,[c] C. Colbeau-Justin,[de] S. Sorgues,[de] L. F. Liotta[f] and L. Palmisano[ab]

Received 15th March 2013,
Accepted 29th April 2013

DOI: 10.1039/c3cp51142a

www.rsc.org/pccp

Catalytic and catalytic photo-assisted hydration of propene to form 2-propanol in gas–solid regime at atmospheric pressure and 85 °C were carried out by using a heteropolyacid (POM) supported on different oxides. Binary materials were prepared by impregnation of $H_3PW_{12}O_{40}$ on different commercial and home prepared supports (TiO_2, SiO_2, WO_3, ZrO_2, ZnO, Al_2O_3). Some of the composites were active both for catalytic and catalytic photo-assisted reactions. The Keggin type POM was completely and partially degraded, when supported on ZnO and Al_2O_3, respectively, and these binary solids always resulted as inactive for both catalytic and catalytic photo-assisted reactions. The supported Keggin POM species played a key role both for the catalytic and the photo-assisted catalytic reactions, due to their strong acidity and ability to form strong oxidant species under UV irradiation, respectively. The contemporary presence of heat and UV light improved the activity of almost all POM supported materials. All materials were characterized by X-ray diffraction (XRD), scanning electron microscopy observations (SEM), diffuse reflectance spectroscopy (DRS), determination of the conduction and valence band energy by photovoltage measurements, Fourier transform infrared spectroscopy (FTIR), NH_3-TPD experiments and time resolved microwave conductivity (TRMC).

Introduction

Propene hydration to obtain 2-propanol is a reaction carried out at moderate temperatures (*ca.* 150–200 °C) and pressure (2 MPa) in the presence of an acid catalyst;[1] however the realization of this reaction at ambient conditions is of great interest. The use of heteropolyacids as catalysts for the hydration of propene to 2-propanol in a gas–solid regime has been an object of several patents.[2,3] Heteropolyacids, a kind of polyoxometallates (POMs),[4] are very strong Brønsted acids and efficient oxidants that perform fast and reversible redox multielectronic transformations under mild conditions.[5] Ivanov *et al.* compared the catalytic activity of an acidic zeolite with non-supported and two SiO_2 supported $H_3PW_{12}O_{40}$ (POM) samples for this reaction.[6] Supported POM samples resulted much more active than both the bare POM and the zeolite, substantially due to their stronger acidity. The POM based materials showed significant activity from 100 °C with a maximum activity in hydration at 130 °C. They have also been used as homogeneous photocatalysts: absorption of light (λ = 260 nm corresponding to 4.8 eV) by the ground electronic state of the solubilized POM produces the charge transfer-excited state POM* and it is qualitatively analogous to the absorption of band gap radiation by a solid semiconducting metal oxide producing a transient electron–hole pair.[7] Likewise, substrate oxidation by the excited state of the polyoxometalate is analogous to the corresponding process in semiconductors.[8] In this manner, the heteropolyacid can act not only as a catalyst but also as a photocatalyst, so the additional effect of irradiation on the catalytic system can improve its performance. Several studies have been devoted

[a] "Schiavello-Grillone" Photocatalysis Group. Dipartimento di Energia, Ingegneria dell'informazione e modelli Matematici (DEIM), Università di Palermo, Viale delle Scienze, 90128 Palermo, Italy
[b] Consorzio Interuniversitario la Chimica per l'Ambiente (INCA), Italy. E-mail: giuseppe.marci@unipa.it; Fax: +39 091 23860841; Tel: +39 091 23863737
[c] Dipartimento di Fisica e Chimica, Università di Palermo, Viale delle Scienze, 90128 Palermo, Italy
[d] Université Paris-Sud, Laboratoire de Chimie Physique, UMR8000, Orsay, 91405, France
[e] CNRS, Laboratoire de Chimie Physique, UMR8000, Orsay, 91405, France
[f] Istituto per Lo Studio dei Materiali Nanostrutturati (ISMN)-CNR, via Ugo La Malfa 153, 90146 Palermo, Italy

† Electronic supplementary information (ESI) available: SEM microphotography of Al_2O_3; POM/Al_2O_3; ZnO and POM/ZnO samples along with ZrO_2, 2L-POM/ZrO_2 and POM/ZrO_2. See DOI: 10.1039/c3cp51142a

to heterogeneous photocatalytic processes by using semiconductor oxides. This technology has been applied mainly to degrade organic and inorganic pollutants both in vapour and in liquid phases.[9] The main advantages of photocatalysis consist not only in the mild conditions under which the process can be carried out, but also in the possibility to abate refractory, very toxic and not biodegradable molecules. Many semiconductor oxides such as TiO_2, ZnO and WO_3, that are active under UV irradiation at wavelengths corresponding to or lower than their band-gap, have been tested as photocatalysts.[10,11] Also POM materials, when excited to POM* by light, can work as better oxidant and reductant species with respect to the corresponding ground states.[12] Indeed, POM* can easily become POM^-, a ''heteropolyblue'' species by means of one (or more) electron transfer from another species.[13] Heteropolyblue species ''POM^-'', indicated also as $PW_{12}O_{40}^{4-}$, absorbs visible light at λ = 650 nm, are relatively stable, and are readily re-oxidized to $PW_{12}O_{40}^{3-}$. The photo-reduction of POM is synergistically enhanced by coupling it with TiO_2 which directly transfers photo-generated electrons from the conduction band to interfacial POM with empty d orbitals. In coupled POM/TiO_2 samples, then, the rate of conduction band (CB) electron transfer is enhanced, and consequently the charge-pair recombination is delayed.[14] Enhanced degradation of organic compounds in the UV/TiO_2 process has been reported in the presence of Keggin-type POMs, such for instance $H_3PW_{12}O_{40}$ supported on TiO_2.[14–20] Usually, catalytic photo-assisted reactions are carried out at atmospheric pressure and room temperature because the photonic activation of the photocatalyst does not require heating. Herrmann reports that the true activation energy of the process is nil whereas the apparent activation energy is small (few kJ mol^{-1}) in the temperature range 20–80 °C.[21] By using POM containing solids, polar molecules can strongly interact with POM forming the so-called ''pseudo-liquid'' phase.[5,22]

The dispersion of POMs on solid supports with a high surface area, is, moreover, generally useful because the accessibility to their acid sites, and consequently the catalytic activity, increase. Several supports, such as SiO_2,[23–27] Al_2O_3,[24,28,29] ZrO_2,[30,31] Ta_2O_5 [32] and carbon[23,33] have been used to disperse POM. Silica has been widely favoured as supporting material because it interacts weakly with the Keggin anions preserving their structure. On the contrary, the strong interaction of POM with basic solids as MgO or Al_2O_3, inducing POM decomposition, results in a decline of its acidity.[34] These strong interactions were attributed to the basicity of the support[28] and the detrimental effect of such interactions on the catalytic activity has also been well documented.[27–29]

In a previous paper the catalytic and catalytic photo-assisted activity of the $H_3PW_{12}O_{40}$ POM supported on TiO_2 Evonik P25 and SiO_2 was studied and a beneficial role of the photocatalytically active support on the reaction rate was reported.[35] The contemporary presence of heat and UV light improved the activity of the POM supported materials for the propene hydration reaction and the catalytic photo-assisted reaction occurred at a higher rate than the catalytic one when the solid support was an irradiated semiconductor. In that case, the more significant increase of reactivity was justified by considering the ability of TiO_2 to transfer electrons from the conduction band to the activated POM* species. In this paper catalytic and catalytic photo-assisted activities of $H_3PW_{12}O_{40}$ supported on various acid or basic semiconductor and insulator oxides, *i.e.* TiO_2, WO_3, ZnO, SiO_2, Al_2O_3 and ZrO_2, have been investigated for propene hydration.

Some bulk and surface properties of the materials have been studied and the cooperative effect of light and heat has been investigated by taking into account that the (photo)reactivity can depend on the type of support influencing the POM features.

Experimental

Solid samples used as catalysts and photocatalysts

The solids used as supports for the polyoxometalate were commercial TiO_2 Evonik P25 and TiO_2 Merck, SiO_2 Riedel de Haën, γ-Al_2O_3 Fluka. WO_3, ZnO and ZrO_2 were purchased from Aldrich. A home prepared (hp) TiO_2 sample was prepared by adding titanium isopropoxide (TTIP) to an ethanolic solution containing the pluronic P127. After addition of HCl and H_2O a white solid gel was obtained and it was maintained under stirring at 40 °C for 24 h. Subsequently, the solvent was evaporated and the obtained solid was dried at 110 °C for 24 h and calcined at 500 °C for 24 h. The molar ratio of the reagents $HCl : H_2O : EtOH : F127 : TTIP$ was 0.5 : 15 : 40 : 0.005 : 1.[36]

The binary materials POM/oxide were prepared by impregnating the support with an aqueous solution containing the desired amount of the commercial $H_3PW_{12}O_{40}$ (Aldrich, 10 $m^2 g^{-1}$). During the preparation each suspension was stirred at 50 °C for 1 h, and then the solvent was evaporated. The powder was dried at 85 °C overnight. The POM amount deposited was 50% in weight with respect to the support. The powders used as catalysts and photocatalysts are denoted hereafter as POM/oxide support. Some samples containing a lower amount of heteropolyacid were prepared by depositing $H_3PW_{12}O_{40}$ in quantities corresponding to 9 or 4.5 wt% on TiO_2 Merck, 4 wt% on WO_3 and 5 or 2.5 wt% on ZrO_2. These amounts were chosen to obtain a theoretical coverage of 2 or 1 layers on the surface of the support, as will be discussed in the following. These materials are labelled hereafter 2L-POM/oxide support or 1L-POM/oxide support.

Characterization of the solids

XRD patterns of the powders were recorded at room temperature in a Philips powder diffractometer using the Cu Kα radiation and a 2θ scan rate of 2° min^{-1}. XRD patterns were used to identify the crystal phase, to check possible POM support interactions giving rise to distortion of the POM structure and to evaluate the particle sizes by means of the Scherrer equation (see ESI†).

The textural properties were obtained using a Carlo Erba Sorptomat 1900 instrument. The samples were evacuated at 120 °C for 3 h prior to analysis. The fully computerized analysis

of the N_2 adsorption and desorption isotherms at −196 °C allowed to obtain the specific surface areas (SSA $m^2\ g^{-1}$) of the samples by means of the BET method in the standard pressure range 0.05–0.3 p/p° of adsorption branch. The total pore volume (V_p) was evaluated on the basis of the amount of nitrogen adsorbed at a relative pressure of 0.998, while mesopore size distribution values (mean pore diameter) and mesopore volumes were calculated by applying BJH model in the range of p/p° of 0.1–0.98 of the desorption branch.[37]

The diffuse reflectance spectra (DRS) were recorded in air at room temperature in the wavelength range 800–250 nm using a Shimadzu UV-2401 PC spectrophotometer, with $BaSO_4$ as the reference material.

Infrared spectra of the samples in KBr (Aldrich) pellets were obtained with a FTIR-8400 Shimadzu spectrometer and the spectra were recorded with 4 cm^{-1} resolution and 256 scans.

The ability of the photo-exited POM (POM*) to abstract a photo-generated electron from the conduction band of the semiconductors has been studied by measuring the reduction potential of the conduction band of the semiconductors used as support. These measurements have been carried out by the methodology developed by Bard *et al.*[38,39] and modified by Roy *et al.*[40] This method is based on the pH-dependence of the flat band potential of the semiconductor, that in the case of n-type semiconductors can be assumed to be equal to the potential of the conduction band.[41] For these measurements 100 mg of TiO_2 (hp, Merck or Evonik P25) and 20 mg of methylviologen dichloride (Aldrich) were suspended in 100 ml of 0.1 M $NaNO_3$ solution. The suspension was stirred and bubbled with N_2 prior to and during the measurements in a five necked beaker. The pH was adjusted with HNO_3 and NaOH solutions and monitored by a pH meter during the course of the measurement. An Ag/AgCl electrode was used as the reference and a platinum one as the working electrode. The suspension was irradiated by two 125 W medium pressure Hg lamps.

The acidity of the (photo)catalysts was determined by temperature-programmed desorption of ammonia (NH_3-TPD) experiments by using a Micromeritics Autochem 2910 apparatus equipped with a thermal conductivity detector (TCD) and a mass quadrupole spectrometer (Thermostar, Balzers). The sample amount of 0.3 g was pre-treated in He flow at 200 °C for 1 h. Then, after cooling down to room temperature, ammonia adsorption was performed by admitting a flow of 5% NH_3/He stream (30 ml min^{-1}) for 1 h. In order to remove all the physically adsorbed ammonia, the sample was purged by flowing 100 ml min^{-1} He at 100 °C for 1 h, then after cooling down to room temperature, ammonia desorption was started by flowing He (30 ml min^{-1}) and heating up to 500 °C (rate of 10 °C min^{-1}). All the gases desorbed from the sample were monitored by online TCD and QMS analysis. The total acidity of the catalyst was calculated by integration of the NH_3 desorption profile referred to the QM signal, at mass 15. Such mass value was preferred to the mass signal at 17, in order to exclude any contribution due to water fragmentation.

The charge-carrier lifetimes in bare and POM loaded TiO_2 and WO_3 samples, after UV irradiation, have been determined by microwave absorption experiments using the Time Resolved Microwave Conductivity method (TRMC).[42] TRMC measurements were carried out as previously described.[43] The incident microwaves were generated by a Gunn diode in the K_a band (29–31 GHz). The experiments were performed at 30.0 GHz, frequency corresponding to the highest microwave power. Pulsed light source was a Nd:YAG laser providing an IR radiation at λ = 1064 nm. Full width at half-maximum of one pulse was 10 ns, the repetition frequency of the pulses was 10 Hz. UV light (355 nm) was obtained by tripling the IR radiation. The light energy density received by the sample was 1.3 mJ cm^{-2}. The principle of TRMC and the experimental set-up have been widely described in a previous paper.[43] This technique is based on the measurement of the change of the microwave power reflected by a sample, induced by its laser pulsed irradiation. In the specific case of TiO_2, the TRMC signal can be attributed to electrons because their mobility is much larger than that of the holes. The main data provided by TRMC are given by the maximum value of the signal (I_{max}), which reflects the number of the excess charge-carriers created by the UV pulse, and the decay due to the decrease of the excess electrons controlled by the relaxation time of trapped holes. The understanding of the whole decay is not obvious because various processes are taking place simultaneously. Detailed explanations and interpretations on the decay in TRMC measurements have been published previously.[43,44]

Reactivity experiments

A cylindrical continuous Pyrex photoreactor horizontally positioned (diameter: 10 mm, length: 100 mm) was used and it operated in gas–solid regime. The set-up of the system was reported elsewhere.[35] A porous glass septum in the inlet of the flow allowed to distribute homogeneously the gaseous mixture. The reactivity runs were carried out with 0.5 g of solid powder by simply dispersing it as a thin layer inside the photoreactor (the fixed bed height was *ca.* 0.3 mm). The gas feeding the photoreactor consisted of propene and water with molar concentrations of *ca.* 40 mM and *ca.* 2 mM, respectively. A mass flow controller allowed to feed gaseous propene, whereas water was mixed with the propene stream by means of a home made infusion pump. The flow rate of the gaseous stream for the catalytic and catalytic photo-assisted runs was 20 $cm^3\ min^{-1}$. All the runs were carried out at atmospheric pressure. The reactor and the pipes of the set-up to and from the reactor were heated by an electric resistance and K-type thermocouples allowed to monitor the temperature in the whole system. The reactions were performed at 85 °C. For the catalytic photo-assisted runs the reactor was also illuminated from the top with a Helios-Italquartz 125 W medium pressure Hg lamp. The temperature inside the (photo)-reactor was maintained constant at 85 °C during illumination by means of a refrigeration water jacket surrounding the lamp and a water bath located between the reactor and the lamp filtering the infrared radiations. The irradiance reaching the photoreactor, measured in the range 300–400 nm with a UVX Digital radiometer, was equal to 1.5 mW cm^{-2}. The runs lasted *ca.* 5 h and samples of the

reacting fluid were analyzed by a Shimadzu 17A gas chromatograph equipped with an Alltech AT-1 column and a FID. Some longer runs (10 h) to study the (photo)stablity of the samples were also perfomed.

Results and discussion

Bulk and textural samples characterization

Fig. 1 shows the X-ray diffraction patterns of POM, bare oxides and the supported POM materials. Table 1 summarizes also the main features of the catalysts.

As far as the bare TiO_2 samples is concerned, the various peaks identified correspond to the two main phases of TiO_2, *i.e.* anatase and rutile in the case of Evonik P25 and hp. In the case of TiO_2 Merck only the anatase phase was detected. The ZnO diffraction pattern corresponds to a very well crystalized hexagonal wurtzite structure,[45] whereas ZrO_2 and WO_3 peaks correspond to monoclinic solids. Diffraction patterns of SiO_2 and Al_2O_3 are related to amorphous materials. The features of the XRD diffraction patters of all the impregnated samples (Fig. 1) correspond roughly to those of the bare supports.

No significant changes in the diffraction patterns occurred after the deposition of POM, indicating that POM species are highly dispersed on the support in agreement with previous works[23,35] and also with SEM and EDAX observations. In the POM supported samples on TiO_2 Merck, WO_3 and ZrO_2 new peaks appeared, with respect to the corresponding bare powders.

Table 1 Specific surface area (SSA) and band gap of the oxides used as POM supports

Sample	B.E.T. SSA [$m^2\ g^{-1}$]	Band gap (eV)
TiO_2 Evonik P25	50	3.2
TiO_2 Merck	10	3.2
TiO_2 hp	73	3.0
SiO_2	275	Insulator
WO_3	4	2.6
ZrO_2	5	5.0
Al_2O_3	176	Insulator
ZnO	20	3.2

These new diffraction peaks do not coincide with those observed for the bare POM diffraction pattern and they can be explained by considering the occurrence of a strong interaction POM-support that can introduce distortions within the POM tertiary structure.[22] Table 1 shows the specific surface areas of all of the used supports. TiO_2 hp sample, prepared in the presence of a surfactant showed a higher BET specific surface area (SSA) with respect to those of the corresponding commercial ones. Table 2 includes the SSA values measured for all of the POM supported samples. As a general trend, the surface areas of all of them are smaller than those of the corresponding supports, although the decrease of surface area was not always very significant. In particular, in agreement with previous observations,[24] the decrease of SSA was more important when POM was supported on oxides with a high specific surface area and negligible when it was supported on oxides

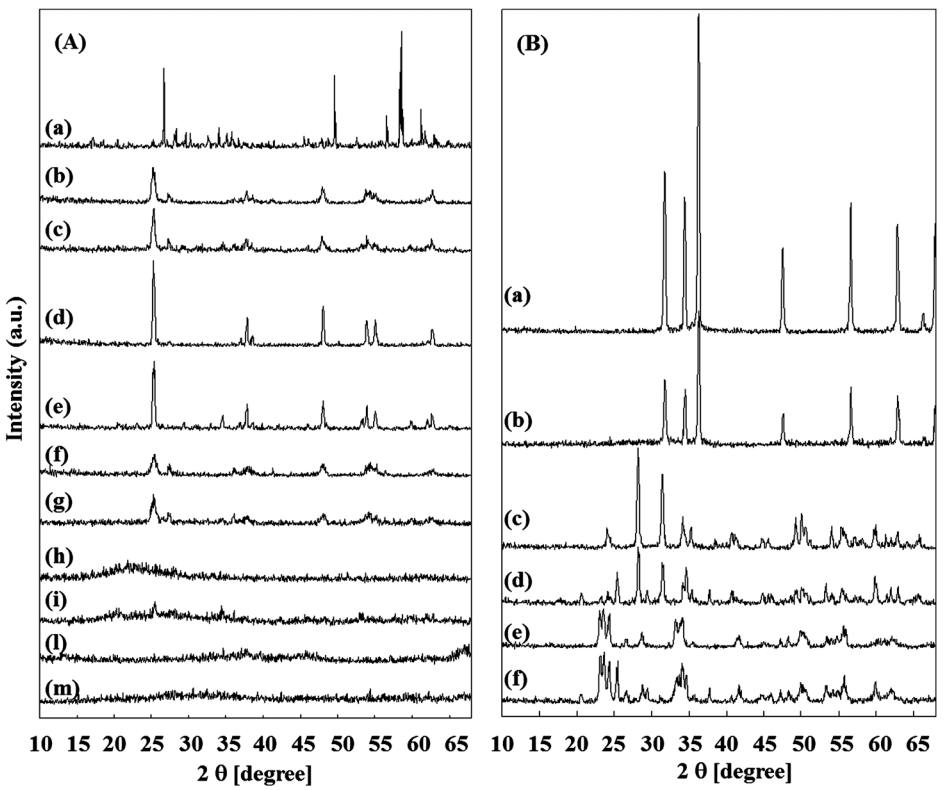

Fig. 1 XRD patterns of the samples (A): (a) bare POM; (b) TiO_2 Evonik P25; (c) POM/TiO_2 Evonik P25; (d) TiO_2 Merck; (e) POM/TiO_2 Merck; (f) TiO_2 hp; (g) POM/TiO_2 hp; (h) SiO_2; (i) POM/SiO_2; (l) Al_2O_3; (m) POM/Al_2O_3; (B): (a) ZnO; (b) POM/ZnO; (c) ZrO_2; (d) POM/ZrO_2; (e) WO_3; (f) POM/WO_3.

Table 2 Atomic percentage of W and of Ti or Si or Zr or Al or Zn, both nominal and measured, specific surface areas (SSA) and theoretical POM coverage on the support for the POM supported samples

Sample	W atomic percentage		Ti or Si or Zr or Al or Zn atomic percentage		B.E.T. SSA [m^2 g^{-1}]	Theoretical coverage [POM layers]
	Nominal	EDAX	Nominal	EDAX		
POM/TiO_2 Evonik P25	13.4	16.1	86.6	83.9	38	2.1
POM/TiO_2 Merck	13.4	18.6	86.6	81.4	10	10
2L-POM/TiO_2 Merck	2.7	0	97.3	100	10	2.0
1L-POM/TiO_2 Merck	1.3	0	98.7	100	10	1.0
POM/TiO_2 hp	13.4	17.3	86.6	82.7	65	1.4
POM/SiO_2	10.4	10.8	89.6	89.2	220	0.40
POM/WO_3	—	—	—	—	7	27
2L-POM/WO_3	—	—	—	—	6	2.0
POM/ZrO_2	19	20	81	80	8	21
2L-POM/ZrO_2	2.3	0	97.7	98.3	8	2.0
1L-POM/ZrO_2	1.2	0	98.8	100	8	1.0
POM/Al_2O_3	8.9	—	91.1	—	110	0.60
POM/ZnO	13.5	—	86.5	—	5	5.3

with low SSA. The amount of POM supported on the oxides with high surface areas (SiO_2 and Al_2O_3) was probably sufficient to block a fraction of pores, according to the literature reporting such an effect for mesoporous supports, due to a heteropolyacid.[46] Values of the surface area, total pores volume, mesopores volume and diameter for two selected POM supported samples, *i.e.* POM/TiO_2 hp and POM/SiO_2, are reported in Table 3 and they can be compared with the figures obtained for corresponding oxides used as supports (see Table 1).

As expected, the total pores volume of silica was more than double with respect to TiO_2, although the pores diameter was virtually identical. This finding suggests that for silica the greatest part of the surface area is due to a contribution from mesopores. The more pronounced decrease of the surface area and in particular of the pore volume and pore diameter observed after POM loading on SiO_2 suggests, as already reported,[47–49] that POM deposition occurs mainly inside the pores. On the contrary, over the less porous TiO_2 hp, POM likely grows layer by layer resulting in a little effect on the surface properties of the support. SEM microphotographs for the TiO_2 based materials are reported in Fig. 2(a)–(f). The morphologies of the POM/TiO_2 Evonik P25 particles are very similar to that of the bare TiO_2 Evonik P25 used as support (SEM microphotograph of bare TiO_2 P25, here called Evonik P25, has been already reported in a previous paper[35]), since the agglomerates of these particles present the same shape and consist of nanoparticles with similar sizes (*ca.* 30–40 nm). As far as TiO_2 Merck is concerned, the samples with lower POM amount (9% and 4.5%), *i.e.* 2L-POM/TiO_2 Merck and 1L-POM/TiO_2 Merck, showed an identical morphology of the bare support (agglomerates of particles with sizes ranging between 90 and 200 nm). On the contrary, SEM observation of the POM/Merck catalyst showed zones where the nanoparticles seem merged by the presence of POM, reaching sizes up to *ca.* 600 nm. Negligible differences can be noticed between the TiO_2 hp and POM/TiO_2 hp samples that appeared as agglomerates of particles with sizes ranging between *ca.* 20–25 nm. Table 2 reports the nominal and the average EDAX values of the atomic percentage of W from POM and the atomic percentage of metal or silicon from the support calculated by taking into account the presence of thirteen water moles in 1 mole of POM.[50] A quite homogeneous distribution of POM on the surface of both TiO_2 Evonik P25 and POM/TiO_2 hp samples was evidenced. No tungsten was observed by EDAX for the 2L-POM/TiO_2 Merck and 1L-POM/TiO_2 Merck, due to the fact that the amount of tungsten was very low (nominal 2.7 and 1.3%, respectively). For POM/TiO_2 Merck sample, EDAX analyses evidenced the presence of POM agglomerates on the TiO_2 surface. In fact, significant oscillation of the experimental percentages of tungsten with respect to the nominal one was found by analyzing several particles. For this sample tungsten on the surface appears to be not homogeneously spread. Fig. 2 also reports selected SEM microphotographs of the SiO_2 and WO_3 based materials (Fig. 2(g)–(k)). Slight enlargement of the nanoparticles constituting the agglomerates for POM/SiO_2 can be observed. The interstitial spaces between the bare SiO_2 particles almost disappeared. This insight could explain the surface area decrease for the POM/SiO_2 material with respect to the bare SiO_2. The amount of tungsten from POM measured by EDAX analyses resulted as almost equal to the nominal one (Table 2).

The sample 2L-POM/WO_3 with lower POM amount (4%) showed the presence of zones where the WO_3 nanoparticles (sizes ranging between 70 and 130 nm) seem to be merged due to the presence of POM. This fact is even more evident for the sample with the highest amount of POM and suggests that for both 2L-POM/WO_3 and POM/WO_3 samples the distribution of POM was not uniform on the WO_3 surface. As far as ZrO_2 based samples are concerned (SEM micrographs not reported for the sake of brevity, see ESI†), the samples with lower POM amount (2L-POM/ZrO_2 and 1L-POM/ZrO_2) showed an identical morphology of the bare support. Moreover, due to the fact that the amount of W was very low (nominal 2.3 and 1.2%, respectively), no tungsten was observed by EDAX for these samples. On the contrary, the sample POM/ZrO_2 showed zones where the nanoparticles seem to be merged by the presence of POM. In this case EDAX analyses evidenced that POM was not uniformly distributed on the surface of the support as a very large

Table 3 Comparison between morphological properties of two POM supported samples and the corresponding carrier oxides

Sample	B.E.T. SSA (m^2 g^{-1})	Total pores volume[a] (cm^3 g^{-1})	Mesopores volume[b] (cm^3 g^{-1})	Mesopores mean diameter[b] (nm)
TiO_2 hp	73	0.30	0.27	10.0
POM/TiO_2 hp	65	0.27	0.23	9.8
SiO_2	275	0.75	0.71	9.6
POM/SiO_2	220	0.56	0.52	7.7

[a] Determined from a single point of adsorption at p/p° = 0.998. [b] Determined by applying BJH model in the range of p/p° 0.1–0.98 of desorption branch.

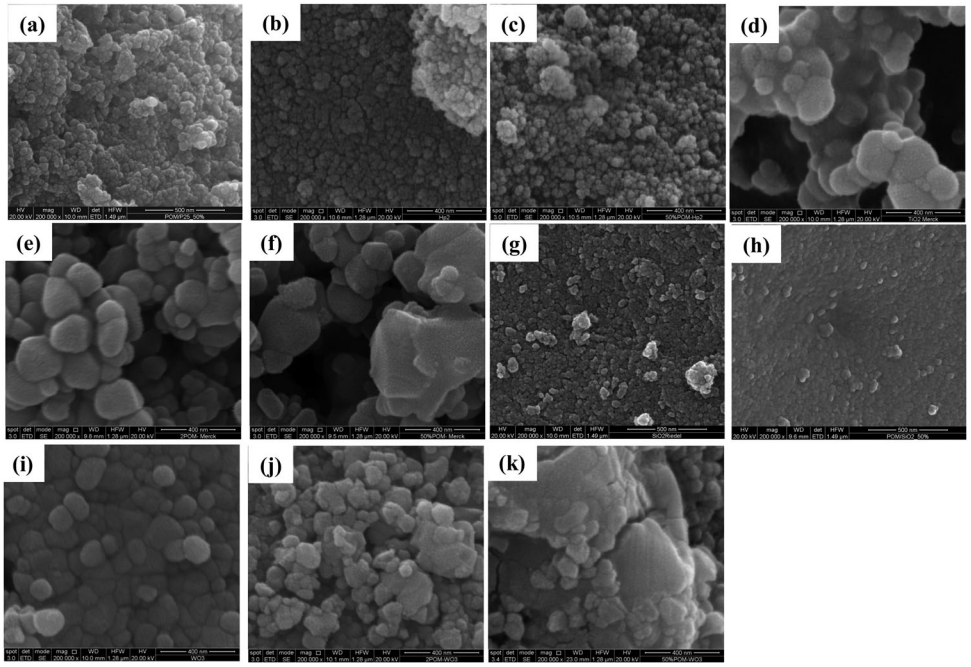

Fig. 2 SEM microphotographs for (a) POM/TiO_2 Evonik P25; (b) TiO_2 hp; (c) POM/TiO_2 hp; (d) TiO_2 Merck; (e) 2L-POM/TiO_2 Merck; (f) POM/TiO_2 Merck; (g) SiO_2; (h) POM/SiO_2; (i) WO_3; (j) 2L-POM/WO_3; (k) POM/WO_3.

scattering on the W atomic percentage values was obtained (from 13 to 30%).

Notably, however, the average value for the W atomic percentage, as reported in Table 2, is almost identical to the nominal one. In the case of the POM/Al_2O_3 and POM/ZnO samples, due to the fact that POM was degraded by the support (see FTIR analyses), these materials were not active as catalysts and consequently only a morphological study was carried out. From SEM observations, not reported for the sake of brevity (see ESI†), it is evident that the morphology of POM/Al_2O_3 is virtually identical to that of Al_2O_3, whereas the presence of POM causes merging of the ZnO particles in POM/ZnO sample.

Fig. 3 reports the diffuse reflectance UV-Vis spectra (DRS) of the bare TiO_2 and POM/TiO_2 supported samples. In particular, Fig. 3(A) reports the DRS of commercial bare and POM supported TiO_2 samples along with the bare $H_3PW_{12}O_{40}$ spectrum. The commercial POM showed a strong UV absorption attributed to the charge transfer from O 2p to W 5d which occurred at the W═O bonds of the Keggin unit at *ca.* 190 nm (not shown) and a weaker band at approximately 260 nm corresponding to a charge transfer in the W–O–W bonds of the units.[7] Inset in Fig. 3(A) shows the absorbance of some selected samples reported in Fig. 3.

A wide band can be observed for the bare heteropolyacid in the range 300–360 nm, in agreement with Pizzio *et al.*[23] This wide band, observed only for the optical characterization of the solid POM material, is responsible for the location of the band edge of the bare POM at wavelengths higher than those expected (260 nm). As far as the TiO_2 samples are concerned, the charge transfer process from O 2p to Ti 3d corresponding to the band gap values, *ca.* 3.2 eV for anatase and 3.0 eV for rutile, can be identified (see the strong absorption in the range 250–380 nm). TiO_2 is an indirect semiconductor[51] and the band gap energies of the samples have been estimated (see Table 1) from the tangent lines in the plots of the modified Kubelka–Munk function, $[F(R'_\infty)h\nu]^{1/2}$, *versus* the energy of exciting light.[52]

For POM/TiO_2 Merck the DRS does not change significantly with respect to that of the bare TiO_2. On the contrary, the spectrum of the POM supported on Evonik P25 redshifts closer to the bare POM.[35,53] These observations could be related to a different interaction between POM and the two types of TiO_2.

A red-shift has been reported for samples containing POM species on TiO_2 surface.[16] It seems that POM has a shielding effect only when present on the surface of TiO_2 Evonik P25 and for this reason the DRS of POM/TiO_2 Evonik P25 moves towards that of bare POM. On the contrary the negligible DRS shift with respect to that of the starting TiO_2 observed in the case of POM/TiO_2 Merck sample, suggests that the optical properties of POM are strongly influenced by the presence of TiO_2 Merck. In Fig. 3(B) a blue-shift towards the DRS spectrum of bare POM was observed for POM/TiO_2 hp with respect to the TiO_2 hp spectrum and a red-shift towards the DR spectrum of bare POM was observed for POM/ZnO with respect to the ZnO spectrum. These findings can be explained by considering the same POM shielding effect evocated in the case of POM/TiO_2 Evonik P25 sample. Moreover the DRS of ZnO showed the typical broad absorption band that can be ascribed to the charge transfer process from O^{2-} to Zn^{2+} responsible for the ZnO band gap that has been estimated[54] to be 3.2 eV in agreement with previous measurements.[55,56]

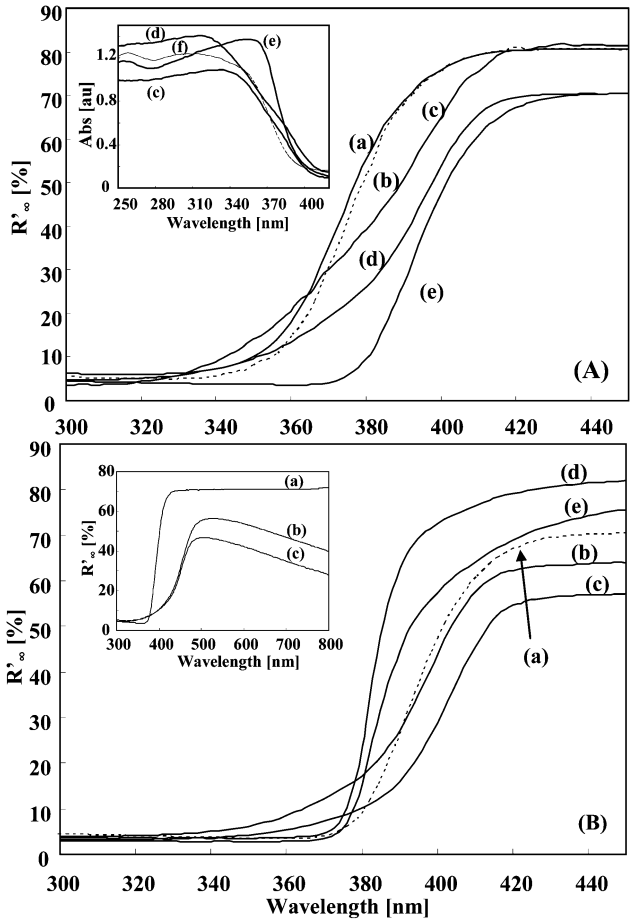

Fig. 3 Diffuse reflectance spectra of (A): (a) POM/TiO_2 Merck; (b) TiO_2 Merck; (c) TiO_2 Evonik P25; (d) POM/TiO_2 Evonik P25; (e) bare POM. Inset in (A): same as in the figure and (f) POM after 24 h at 100 °C and (B): (a) bare POM, (b) POM/TiO_2 hp; (c) TiO_2 hp; (d) ZnO; (e) POM/ZnO. Inset in (B): (a) bare POM; (b) WO_3; (C) POM/WO_3.

From the perusal of the inset of Fig. 3(B) it can be concluded that, analogously to the case of POM/TiO_2 Merck, the DRS of POM/WO_3 does not significantly change with respect to that of the bare WO_3, indicating also in this case that the optical properties of POM are strongly influenced by the presence of this oxide.

In Fig. 4 the POM/Al_2O_3, POM/ZrO_2 and POM/SiO_2 diffuse reflectance spectra along with that of bare POM are reported. Due to the fact that the above bare support oxides can be considered insulators, the observed spectra of POM supported samples are due to the presence of POM.

The determination of the flat band potential, that in the case of n-type semiconductors can be assumed to be equal to the potential of the conduction band,[41] was performed on the TiO_2 bare samples (Evonik P25, Merck and hp). The pH dependence of the potential of a platinum electrode in the presence of an electron acceptor (methylviologen dichloride, MV^{2+}) with a pH-independent reduction potential was recorded in a UV irradiated semiconductor suspension. According to the method developed by Roy *et al.*,[40] the flatband potentials (E_{fb}) of the different semi-conductors have been obtained by recording the

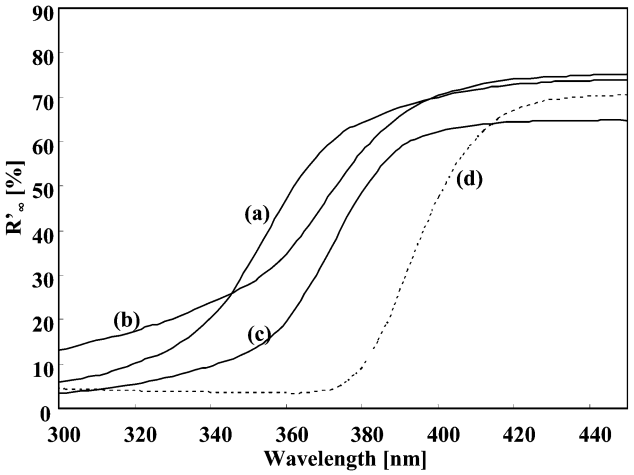

Fig. 4 Diffuse reflectance spectra of (a) POM/Al_2O_3; (b) POM/ZrO_2; (c) POM/SiO_2; (d) bare POM.

photovoltage in the presence of MV^{2+}. When a semiconductor suspension is irradiated by light with a suitable wavelength, the Fermi level (E_f) splits into two quasi-Fermi levels, one for the holes (h_{VB}^+) and one for the electrons (e_{CB}^-). The quasi Fermi level for the electrons ($E_f(e^-)$) practically merges with the conduction band of the semiconductor, and therefore:

$$E_{f(e^-)} \cong E_{CB} \cong E_{fb} \quad (1)$$

In the presence of methylviologen, the excited electrons are trapped by MV^{2+} to form MV^+:

$$e_{CB}^- + MV^{2+} \rightleftarrows MV^+ \quad (2)$$

and $E_{f(e^-)}$ will equilibrate with the Fermi level of the redox couple in solution:

$$E_{f(e^-)} = E_{fb} = E_{f(MV^{2+}/MV^+)} \quad (3)$$

The E_f of the semiconductor varies with the pH of the solution, according to the following equation:

$$E_{f(e^-)} = E_{fb} = E_{fb}(pH = 0) - KpH \quad (4)$$

where $E_{fb}(pH = 0)$ is the flatband potential at pH = 0 and K is a constant factor of 0.059 V. By substituting eqn (3) in eqn (4), it can be written:

$$E_{fb} = E_{f(MV^{2+}/MV^+)} = E_{fb}(pH = 0) - KpH = \\ = E^0_{(MV^{2+}/MV^+)} + 0.059 \log\frac{a_{MV^{2+}}}{a_{MV^+}} \quad (5)$$

where $E^0_{(MV^{2+}/MV^+)} = -0.445$ V (*vs.* NHE). Since the redox potential of the MV^{2+}/MV^+ couple is pH independent, any change in the photovoltage as a function of the pH has to be attributed to the changes in the energy of electrons photo-generated at the semiconductor surface. At a low pH value, the electrons generated in the conduction band have not enough power to reduce the methylviologen. By increasing the pH the flat-band potential of the semiconductor decreases and, when it becomes more negative with respect to the redox potential of

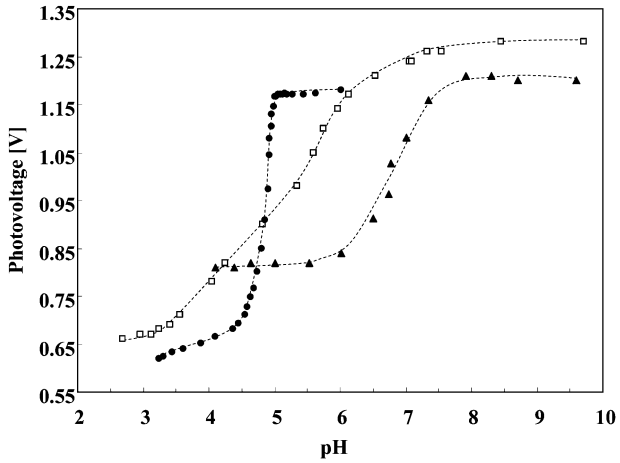

Fig. 5 Photovoltage meausurements *vs.* pH recorded during UV light irradiation in the presence of TiO_2 Evonik P25 (●); TiO_2 Merck (▲) and TiO_2 hp (□).

the couple MV^{2+}/MV^{+}, reduction of the methylviologen occurs. Fig. 5 reports the potential developed at the platinum electrode (E), with respect to the reference one, *versus* the pH of the TiO_2 suspension. In the obtained curve the inflection point indicates the pH at which E_f coincides with $E^0_{(MV^{2+}/MV^{+})}$, *i.e.* the pH value equal to pH_0. Consequently at pH = pH_0, eqn (5) can be written as:

$$E_{fb}(pH_0) = E^0_{(MV^{2+}/MV^{+})} = E_{fb}(pH = 0) - KpH_0 \quad (6)$$

while at any pH:

$$E_{fb}(pH) = E_{fb}(pH = 0) - KpH. \quad (7)$$

A combination of eqn (6) and (7) gives:

$$\begin{aligned} E_{fb}(pH) &= E^0_{(MV^{2+}/MV^{+})} + KpH_0 - KpH \\ &= E^0_{(MV^{2+}/MV^{+})} - K(pH - pH_0) \end{aligned} \quad (8)$$

which allows us to determine the flatband potential at any pH. E_{fb} values at pH = 7 and pH = 0 for the various catalysts used in this work were determined and they are reported in Table 4.

The home prepared TiO_2 seems to have a flatband potential very close to that of the TiO_2 Evonik P25. Moreover, it is worth to note that the flatband potential at pH = 7, obtained for the TiO_2 Evonik P25 semiconductor is in good accordance with that previously obtained by Macyk *et al.*[41] These results confirm that the conduction band energies of the TiO_2 samples are suitable to transfer electrons to the excited POM. It is worth to note that the first reduction potential of the Keggin species, which is independent of the pH value, is equal to +0.226 V.[13]

The samples were also analyzed by FTIR in order to confirm the structural integrity of the Keggin unit after the deposition onto the support. The structure of the $PW_{12}O_{40}^{3-}$ anion consists of a PO_4 tetrahedron surrounded by four W_3O_9 groups formed by edge sharing octahedra.[57] This arrangement gives rise to four stretching bands: P–O stretching mode at 1080 cm^{-1}, W═O stretching observed at 990 cm^{-1} and two peaks at *ca.* 910 and 810 cm^{-1} attributed to two types of W–O–W units.[58] It is difficult to characterize the structures of the composites with IR spectroscopy, because some of these bands are overlapped with the bands of the support.

Fig. 6(A) shows the FTIR spectra of the POM/TiO_2 samples along with the bare POM. For the bare POM (Fig. 6(A) (a)) the four main stretching bands attributed to the vibrations of the skeletal bonds in POM, are clearly visible and are located at the wavelengths reported above. The typical band for P–O stretching mode is displayed along with the W═O stretching. The two peaks attributed to two types of W–O–W units are partially covered by the cut-off of TiO_2 in the POM/TiO_2 samples (Fig. 6A (b–d)). In fact, TiO_2 presents intense and broad vibration peaks originated from Ti–O–Ti bonds located at wavenumbers lower than 900 cm^{-1}. Bands at the same wavenumbers for commercial POM appear also when POM is loaded on the surface of the TiO_2 materials, indicating that the Keggin geometry of POM has still been preserved in the binary material. The only exception is the POM/TiO_2 hp sample where the P–O stretching (1080 cm^{-1}) and the W═O stretching (990 cm^{-1}) are slightly shifted to lower wavelengths indicating an interaction of the Keggin species with the support surface.

The SiO_2 asymmetric and symmetric Si–O–Si stretching vibrations band located at *ca.* 1080 and 800 cm^{-1},[59] respectively, completely overlap two fingerprint vibrations of the $PW_{12}O_{40}^{3-}$ species in the range 1100–700 cm^{-1}; however the W═O stretching vibration at *ca.* 981 cm^{-1} remains the same for all of the samples. Therefore, the spectra indicate that the

Table 4 Flat-band potential for the TiO_2 samples

Sample	pH_0 (inflection point)[a]	E_{fb} (pH = 7, NHE)[b]/V	E_{fb} (pH = 0, NHE)[b]/V
TiO_2 Evonik P25	4.85	−0.57	−0.16
TiO_2 hp	5.00	−0.56	−0.15
TiO_2 Merck	6.80	−0.46	−0.04

[a] Standard deviation less than 0.10. [b] Standard deviation less than 0.02.

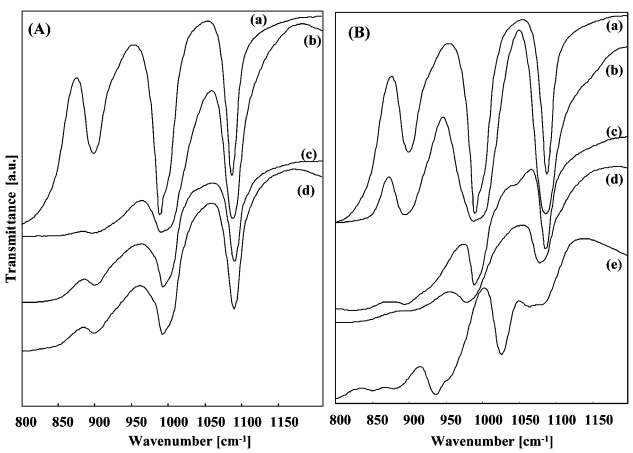

Fig. 6 FT-IR spectra of KBr pellets of (A): (a) bare POM; (b) POM/TiO_2 Merck; (c) POM/TiO_2 Evonik P25; (d) POM/TiO_2 hp and (B): (a) bare POM; (b) POM/ZrO_2; (c) POM/WO_3; (d) POM/WO_3 after reaction; (e) POM/ZnO.

species present in the samples correspond to the commercial POM anion $PW_{12}O_{40}^{3-}$ in agreement with the literature. It is notable that the bands attributed to the Keggin's unit skeletal vibrations did not become more intense in the samples where the POM was supported with respect to those attributed to the bare POM, as expected in the absence of anion–anion interactions. This finding can be explained by considering the relatively low amount of POM and/or its homogeneous dispersion on the support surface. H-bonding interactions cannot be excluded, considering the slight broadening of the bands indicating that the vibrations could be disturbed by dipole–dipole interactions, probably between the Keggin units and the TiO_2 or SiO_2 surface.[60]

The typical FTIR spectrum of the Keggin species was completely absent for the samples POM/Al_2O_3 and POM/ZnO, indicating that the integrity of the POM system was strongly disturbed in agreement with previous studies.[23,28,29] This was attributed to an acid–base reaction between the acidic POM and the basic surface of these supports, as demonstrated by the PZC of the oxides. This strong interaction of POM with the basic metal-oxide support results in a decline of its acidity and the detrimental effect of such interactions on the catalytic activity of the binary material has been well documented.[23,28,29,61] It is worth noting that the analogous FTIR spectra of the POM supported materials after being used for 10 h in catalytic or catalytic photo-assisted reactions, not reported for the sake of brevity, showed no significant differences, in the range 1200–800 cm^{-1}, with respect to the fresh powders indicating that no modifications of the POM Keggin unit occurred after the reactivity.

The point of zero charge (PZC) value of surfaces of the various supports can give an idea of the acidic-basic entity of the surface. The oxides used as supports present a PZC ranging between 2 and 10. These values have already been extensively reported in the literature.[62] The PZC values of the oxide supports correspond to *ca.* 4.5, 2, 0.5, 6.7, 8 and 10.5 for TiO_2, SiO_2, WO_3, ZrO_2, Al_2O_3 and ZnO, respectively. ZnO showed the highest PZC value and notably POM degraded when supported on its surface probably due to a strong acid–base interaction. The same reasoning can be applied to the POM/Al_2O_3 sample. On the contrary when POM was supported on the other oxides presenting acidic or neutral PZC values no degradation of the heteropolyacid was observed.

The acid properties of POM supported samples were evaluated by NH_3-TPD experiments. The results are summarized in Table 5 in terms of mmol of NH_3 desorbed per gram of catalyst. The technique provides information on the total acidity of the solids, without distinguishing between Brønsted and Lewis acidity but accounting for the different strength of acid sites. The TPD curves (as QM signal at mass 15) registered in the range of temperature between room temperature and 600 °C are shown in Fig. 7, where three temperature zones associated to the acid sites strength (weak, medium and strong) can be distinguished according to the literature.[63] No peaks due to weak sites were detected, for any sample. A broad peak, ascribed to medium acid sites, was observed for all samples in the range 200–500 °C. Such peak has different intensity depending on the nature of the support. Finally, a contribution of strong acid sites was found between 500–600 °C. In order to discriminate any contribution to acidity of the supports, NH_3-TPD experiments were also registered for the bare oxides and an evident peak due to medium acid sites along with a broad feature due to strong acid sites were observed only in the case of silica. Therefore, for comparison with the POM supported sample, the ammonia desorption of pure silica was also evaluated (see Table 5 and Fig. 7) and the acidity contribution due to the presence of POM onto SiO_2 is reported in brackets. By comparing the results summarized in Table 5 it is evident that the acid sites strength due to the POM is different for the various samples and in particular the catalysts that present the strongest acidity are POM/ZrO_2, POM/WO_3, and POM/TiO_2 Merck. This fact, that is related to the stronger interaction between POM and the support, will be very useful to explain the higher reactivity observed for these catalyst.

Table 5 Acid properties of POM supported catalysts as determined by NH_3-TPD profiles

Sample	T (°C) = 200–500 °C V_{NH_3} (mmol g_{cat}^{-1})	T (°C) = 500–600 °C V_{NH_3} (mmol g_{cat}^{-1})
POM/TiO_2 hp	0.53	0.27
POM/TiO_2 P25	0.49	0.33
POM/TiO_2 Merck	0.09	0.45
POM/SiO_2	0.53 (0.22)[a]	0.52 (0.31)[a]
SiO_2	0.31	0.21
POM/WO_3	0.05	0.57
POM/ZrO_2	0.12	0.67

[a] Acid values of POM/SiO_2 corrected by the contribution of bare silica support.

The TRMC signal gives information of the lifetimes of charge carriers created on a semiconductor by analysis of the maximum value of the signal (I_{max}), of the short range decay (from 0 to 40 ns) corresponding to recombination phenomena, and of the long time range decay (from 40 ns to 5 μs), corresponding to

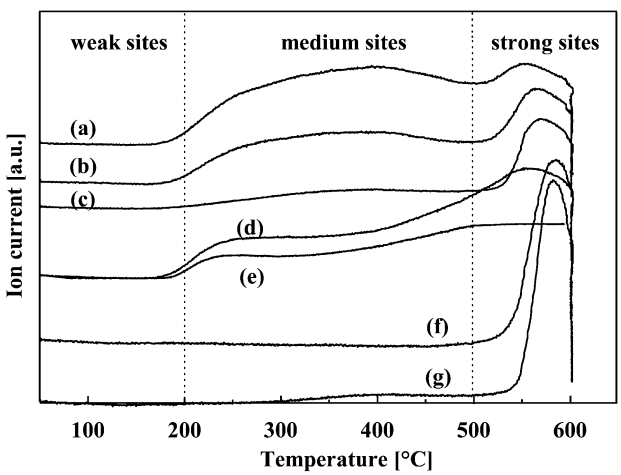

Fig. 7 NH_3-TPD profiles as QM signal at mass 15 for (a) POM/TiO_2 hp; (b) POM/TiO_2 Evonik P25; (c) POM/TiO_2 Merck; (d) POM/SiO_2; (e) SiO_2; (f) POM/WO_3 and (g) POM/ZrO_2.

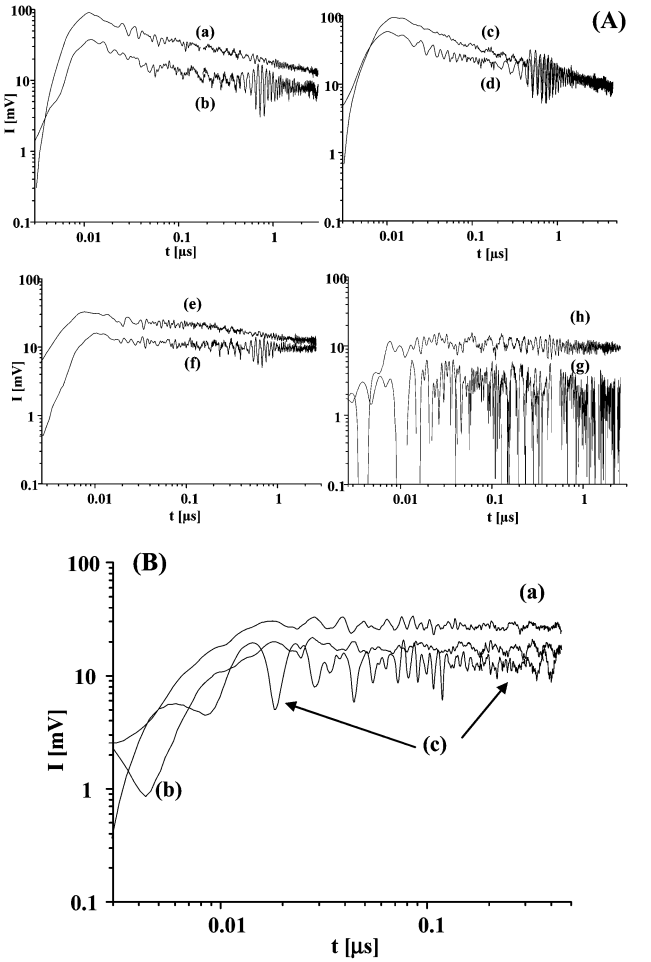

Fig. 8 (A) Compared TRMC signals of support and POM/support: (a) TiO_2 hp and (b) POM/TiO_2 hp, (c) TiO_2 Evonik P25 and (d) POM/TiO_2 Evonik P25, (e) WO_3 and (f) POM/WO_3, (g) SiO_2 and (h) POM/SiO_2. (B). TRMC signals of bare POM (a) first, (b) second and (c) third measurement.

trapping phenomena.[44] Fig. 8 displays the TRMC signals obtained for some selected samples, both bare oxides and POM supported materials. The signals are displayed in double logarithmic plot to observe the decay from the beginning of the laser pulse to 5 μs.

Fig. 8(A) shows the compared TRMC signals obtained for support and POM/support for TiO_2 (both Evonik P25 and hp), WO_3 and SiO_2. The signals were similar for the two kinds of TiO_2 (P25 and hp), that show high I_{max} values (*ca.* 100 mV), but the average signal value for WO_3 was much lower (*ca.* 30 mV). Fig. 8(A) also reports that for SiO_2 no signal was observed.

Fig. 8(B) evidences that bare POM presents a small signal (20 mV), which was not very stable. For this last sample, the TRMC signal has been measured 3 times, and the second and third measurements are slightly lower. This insight can be attributed to the POM degradation by the laser pulse.

In the TMRC signal measured with the POM supported samples on TiO_2 and WO_3 (Fig. 8(A)), the effect of the deposited POM on the signal is identical. The I_{max} is lowered by the presence of the POM and the short-range decay is slightly accelerated.

This indicates that the POM acts like a surface impurity, helping recombination, like in the case of the metallization,[44] but the dominant effect is the influence on the long-range decay, which is, in those three cases showed in Fig. 8(A), slowed down.

The POM has a favorable effect on charge carrier separation. The influence is more important on the TiO_2 Evonik P25 and WO_3, and less significant on the TiO_2 hp. As above-mentioned, bare SiO_2 presents no TMRC signal and the observed one for the POM/SiO_2, reported on Fig. 8(A), may be ascribed to the POM itself or to the injection of charges on SiO_2 by the POM. These results demonstrate that the POM may have an interesting influence on catalytic activity under illumination.

(Photo)reactivity experiments

Neither catalytic nor photo assisted catalytic activity was observed in the presence of the bare oxide materials under the same experimental conditions carried out for the catalytic and catalytic photo-assisted runs. Consequently, it can be concluded that POM is the catalytic species and its presence is needed for the occurrence of propene hydration reaction both in the catalytic and in the catalytic photo-assisted process.

Fig. 9 reports the 2-propanol formation rate for catalytic and catalytic photo-assisted reactions by using the bare POM and the POM supported materials.

The formation of 2-propanol in the presence of POM/ZnO and POM/Al_2O_3 resulted negligible. This behaviour, in agreement with previous observations,[23,28,29,61] was due to the POM decomposition when supported onto these two oxides. This fact confirms that the presence of the Keggin POM species is needed as catalyst and/or photo-catalyst for the hydration propene reaction. By comparing the samples with the highest amount of POM percentage (50%) it was observed that the supported samples on the oxides with higher SSA exhibited higher reactivities, which were higher than that observed for the bare POM. This finding can be related to the fact that the higher the surface area of the support the better the dispersion of the POM onto the surface. Table 2 reports the theoretical POM coverage on each oxide surface by considering the dimension of the Keggin species as 1.2 nm^2.[22]

Of course, the higher the support surface area, the lower the number of theoretical layers of POM on the surface by assuming a homogeneous coverage. For instance, by comparing the catalytic activity of POM supported on TiO_2 materials (50% weight POM on respect to TiO_2), the observed order in activity is: POM/TiO_2 hp > POM/TiO_2 Evonik P25 > POM/TiO_2 Merck. For the same reason also the reaction rate significantly increased with respect to the bare POM material by using the POM/SiO_2 sample. Also POM/ZrO_2 showed an improvement in the reaction rate on respect to the bare POM, although not so significant, probably due to the lower SSA of the support that implies the presence of a *ca.* 21 theoretical layers of POM, that means a thick deposition of Keggin units on the surface of the oxide and hence the behaviour of the POM supported material can be similar to that observed by using the bare POM.

From Fig. 9, by comparing the reactivity of the samples containing the same amount of deposited POM, the most active

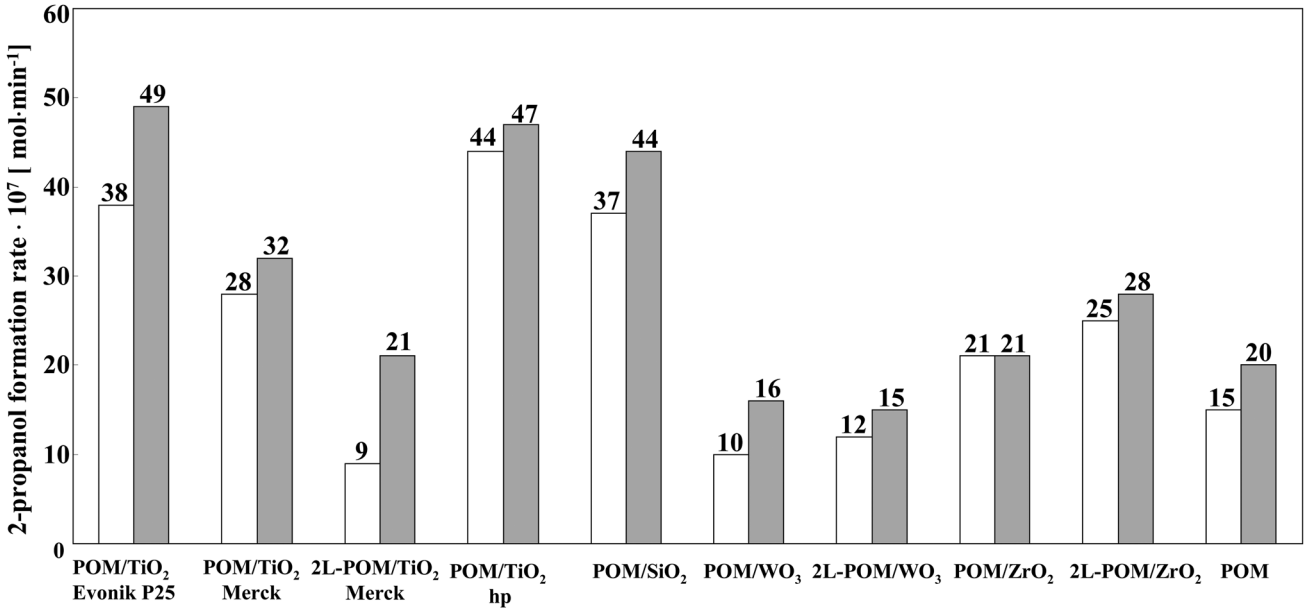

Fig. 9 2-Propanol formation rate by using the various POM supported materials for the catalytic (white bars) and catalytic photoassisted (grey bars) propene hydration reaction.

ones are those with the lowest theoretical POM coverage (see Table 2). For this reason in the case of samples that presented higher theoretical POM coverage *i.e.* POM/TiO_2 Merck, POM/WO_3 and POM/ZrO_2, a set of samples with lower amounts of POM (9, 4, 5 weight percentages, respectively) was prepared, corresponding to two theoretical layers of POM as for the sample POM/TiO_2 Evonik P25 (see Table 2). Moreover, two other samples labeled 1L-POM/TiO_2 Merck and 1L-POM/ZrO_2 with only 1 theoretical layer of POM on TiO_2 Merck or on ZrO_2 were prepared. By comparing the POM supported samples with two theoretical layers on the oxide (Fig. 9) it can be noticed that the activity of 2L-POM/TiO_2 Merck decreases with respect to that shown by POM/TiO_2 Merck and was also lower than that of bare POM. On the contrary, the activity of 2L-POM/ZrO_2 increases with respect to that of the POM/ZrO_2. These behaviours can be due to two opposite effects: the first due to the fact that samples with two layers contain less POM and the second related to the increased dispersion of POM in the samples in comparison with those containing an amount of 50 wt%. In particular, the first effect is predominant in the case of the Merck based material and justifies the reduction of activity. On the contrary, in the case of POM/ZrO_2 the second effect makes that the reactivity not only does not decrease but even increases.

The same considerations can explain the small variation of reactivity in the case of WO_3 based materials in which the two above mentioned effects seem to be balanced. In the case of the 1L-POM/TiO_2 and 1L-POM/ZrO_2 samples, the amount of POM was so small that the first effect was predominant and the reactivity decreased to 5.0×10^{-8} and 8.3×10^{-7} mol min^{-1}, respectively, for the catalytic reaction and to 1.1×10^{-7} and 10×10^{-7} mol min^{-1}, respectively, for the catalytic photo-assisted one.

We can conclude that the support clearly plays a role to improve the catalytic activity of the POM. The higher the SSA of the support the higher the catalytic activity probably because the dispersion and/or coverage of the POM on the surface reach an optimum value. However, the SSA of the support, and hence the coverage of the POM on the oxide, seems not to be the unique parameter influencing the reactivity. In fact, TiO_2 hp and TiO_2 Evonik P25 with a SSA much lower than SiO_2 show a higher or similar reactivity. This fact is probably due to the interaction between the oxide and POM that gives rise to a higher amount of strong acid sites on the POM/TiO_2 hp and POM/TiO_2 Evonik P25 with respect to the POM/SiO_2 (see NH_3-TPD study). Analogously, it is possible to explain the different reactivity observed in the presence of ZrO_2 and in the presence of WO_3 supported powders which have comparable SSA.

From the above discussion, POM appears to be the catalytic species needed for the occurrence of the propene hydration. Consequently the comparison of the catalytic activity of samples containing different amounts of heteropolyacid should be done by using the actitvity normalized for gram of POM present in the catalyst. These values are reported in Fig. 10.

From the perusal of Fig. 10 the most active samples are those which have two layers of POM and in particular the best one is 2L-POM/ZrO_2 followed by 2L-POM/WO_3, 2L-POM/TiO_2 Merck and POM/TiO_2 Evonik P25. The last two samples show very similar catalytic activity. The samples with less POM layers reported in Fig. 10, *i.e.* POM/TiO_2 hp and POM/SiO_2, display reactivity comparable to that of 2L-POM/TiO_2 Merck and POM/TiO_2 Evonik P25. On the contrary, the samples in which a higher number of POM layers were present (POM/TiO_2 Merck, POM/ZrO_2 and POM/WO_3) showed the lowest reactivity.

This finding clearly indicates that two factors influence the reactivity per gram of catalytic species, *i.e.* the POM dispersion and the nature and physico-chemical features of the support. The 1L-POM/TiO_2 Merck and 1L-POM/ZrO_2 samples deserve a

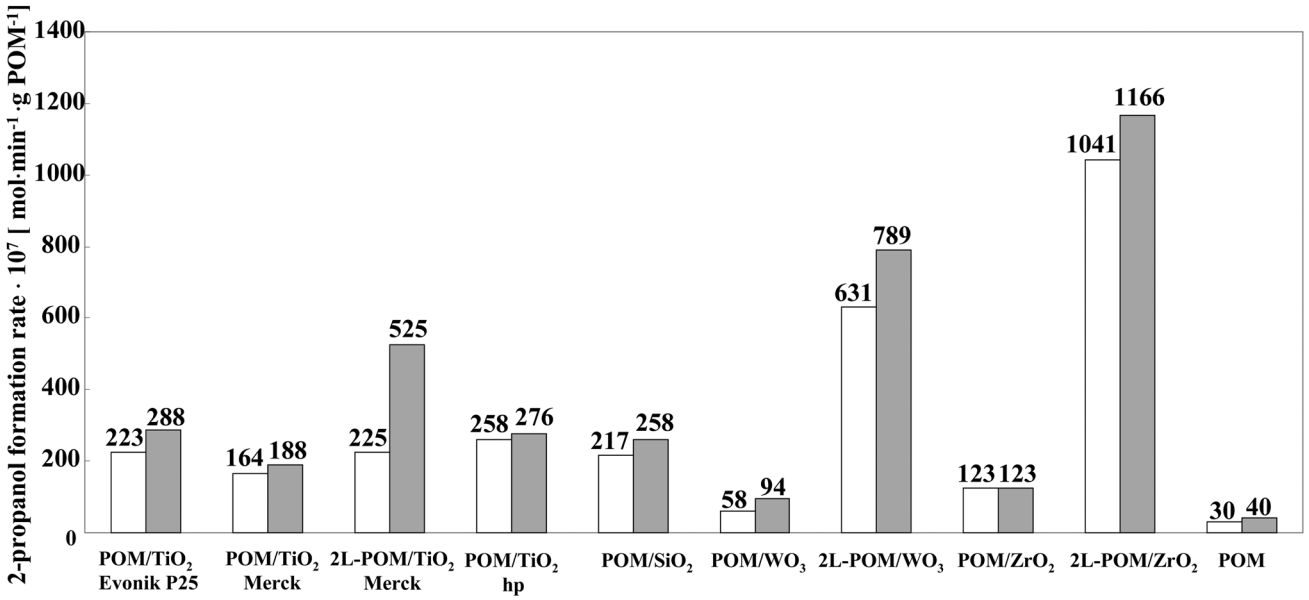

Fig. 10 2-Propanol formation rate per gram of POM present in the various POM supported materials for the catalytic (white bars) and catalytic photoassisted (grey bars) propene hydration reaction.

separate mention. Indeed, for the first one the reactivity per gram of POM drammatically decreased (25×10^{-7} and 55×10^{-7} mol min^{-1} g^{-1} for the catalytic and for the catalytic photo-assisted reaction, respectively) with respect to that observed in the case of the 2L-POM/TiO_2 Merck sample and, on the contrary, for the second one the reactivity decreased only slightly (692×10^{-7} and 792×10^{-7} mol min^{-1} g^{-1} for the catalytic and for the catalytic photo-assisted reaction, respectively) with respect to that observed in the case of the 2L-POM/ZrO_2 sample. In these cases reactivity decreased probably because samples with one theoretical layer of heteropolyacid contain a very low amount of POM.

All the considerations and trends reported for the catalytic runs are valid for the catalytic photo-assisted experiments as well; however it is very important to underline that in almost all cases the reactivity increased in the presence of UV light.

To explain the different catalytic reactivity observed for the various samples it should be considered that the hydration of propene occurs by an acid–base mechanism involving the dioxonium ions situated between POM anions.[6,35] This mechanism could be affected by the acidity of the samples and this hypothesis is effectively confirmed by the NH_3-TPD measurements indicating that POM supported on ZrO_2, WO_3 or TiO_2 Merck samples were those with the strongest acid sites. As far as the catalytic photo-assisted reactions are concerned, in addition to the previous mechanism, a further key role is played by POM being photosensitized to POM* upon exposure to near UV light (see introduction). POM* has a strong oxidation power and can receive an electron from propene being reduced to a blue species (POM^-)[35] (notably the supported POM sample became of blue color in our system under irradiation). Propene carbocation formed coordinates a water molecule from the dioxonium species, hence transferring the positive charge to the oxygen atom. Successively (POM^-) is re-oxidized to the starting (POM) species while one proton is reduced forming a bond with a carbon of the produced propanol. In a previous paper where POM supported SiO_2 and POM supported TiO_2 Degussa P25 samples were tested, the different beneficial influence of light on photoreactivity was explained by considering the occurrence of a synergistic effect only in the coupled POM/TiO_2 sample. Indeed the photoexcited (POM*) possesses an oxidation power ($E^0_{POM/POM^-} = +0.226$ V at any pH) sufficient to abstract a photogenerated electron from the conduction band of TiO_2. Such an electron transfer could play two roles: (i) production of a higher number of (POM^-) species inducing an increase of the reaction rate of 2-propanol formation and (ii) inhibition of the fast electron–hole recombination on TiO_2, as confirmed by TMRC measurements. Interestingly the results reported in Fig. 10 indicate that the increase of reactivity was also high when POM was supported onto an oxide that can not be excited under the used irradiation (ZrO_2) or onto an oxide that can be excited (WO_3) but with a conduction band unable, at least at pH < 3, to inject electrons to POM* (CB potential = +0.40 V at pH = 0). Moreover, as the excitation of POM to POM* occurs at $\lambda \leq 260$ nm (not present in our system), it can be hypothesized that the improvement of photoreactivity under irradiation of POM supported samples can also be due to a modification of the structural properties of POM with an influence on its electronic properties, allowing its photo-excitation also in the presence of light at $\lambda > 260$ nm. A stronger interaction related also with the acidity of the samples could give rise to POM excitation at lower energy. The results indicate that the 2L-POM/ZrO_2, 2L-POM/WO_3 and 2L-POM/TiO_2 Merck samples show the best performances probably because they present stronger interactions evidenced by a higher acidity with respect to the other samples, as NH_3-TPD measurements indicate.

On the other hand XRD analysis suggests the presence of a distorted POM structure only for these samples. The fact that the 1L-POM/TiO_2 Merck and 2L-POM/TiO_2 Merck samples present the highest increase of reactivity in the presence of light indicates that also the electron transfer from the CB of TiO_2 to POM plays a role. Similarly we can explain the high increase of reactivity in the presence of light for the 2L-POM/WO_3 sample. Indeed for this catalyst the TMRC measurements indicate that electron transfer from the CB of WO_3 to POM can occur, probably because the WO_3 surface possesses suitable acidic surface properties.

During the catalytic and catalytic photo-assisted experiments along with the 2-propanol formation reaction also the formation of di-isopropylether occurred. It is worth noting that the selectivity of the reaction *versus* 2-propanol or di-isopropylether is strongly affected by the amount of water in the gas feeding as already reported by Ivanov *et al.*[6] for a catalytic propene hydration by using POM supported on SiO_2. Both for catalytic and catalytic photo-assisted reactions, in general, by increasing the amount of water the selectivity to 2-propanol increases and that to di-isopropylether decreases. Generally speaking, an optimum in water content was observed; indeed, when further increasing the water a decrease in the reaction rate was observed, probably because water competed with propene for adsorption on the catalytic sites.[6]

By using the POM supported on all the oxides and with the water amount in the current experimental conditions, the reaction rate of di-isopropylether formation, both in the absence and presence of UV light, was generally much more lower (by one order of magnitude) than that of the 2-propanol formation. Only in the case of the runs carried out in the presence of POM/TiO_2 Evonik P25, POM/TiO_2 hp and POM/SiO_2 samples the formation rate of di-isopropylether was comparable, but always lower (by *ca.* a half), than that of 2-propanol formation. This last finding, due to the fact that the formation of di-isopropylether is favored in the presence of a lower amount of water, could indicate that the TiO_2 Evonik P25, TiO_2 hp and SiO_2 supports adsorb more efficiently the water present in the gas feeding. This field will be focused in a future work and it is out of the aim of the present work.

The TRMC results may explain the differences observed in Fig. 9 and 10 between catalytic and catalytic photo-assisted results. The influence of the photons on the catalytic reaction may be related to the influence of the POM on the charge-carrier lifetimes of the catalyst. The observed slower decays on POM/Evonik P25 and POM/WO_3 compared to bare supports may be related to a stronger effect of photons on the catalytic reaction. On the other hand, POM did not really influence the charge carrier of hp compound and the photons had no strong effect on the catalytic reaction of POM/TiO_2 hp. It may also be noted that the evidenced injection of charge-carriers by the POM on SiO_2 may explain the better activity of the POM/SiO_2 catalyst under illumination.

Conclusions

The hydration of propene to 2-propanol in a gas–solid regime was successfully carried out at atmospheric pressure and 85 °C by using a heteropolyacid (POM) supported on different oxides in a (photo)catalytic system. Binary materials were prepared by impregnation of $H_3PW_{12}O_{40}$ on different commercial and home prepared supports (TiO_2, SiO_2, WO_3, ZrO_2, Al_2O_3, ZnO). The supported Keggin POM species played a key role both for the catalytic and the photo-assisted catalytic reactions, due to their strong acidity and ability to form strong oxidant species under UV irradiation, respectively. The role of the support should also be considered to explain the different catalytic reactivity of the various samples. In particular, the SSA of the support and the interaction with POM, that can enhance the superficial acidity of the samples, play an important role in the catalytic reactivity of the samples. Indeed, it was observed that the supported samples on the oxides with higher SSA exhibited higher reactivities. This finding can be related to the better dispersion of the POM on the catalyst surface. Moreover, as evidenced by comparing the samples reactivity per gram of supported POM, the most active materials were those that presented the strongest acid sites (see NH_3-TPD measurements), *i.e.* ZrO_2, WO_3 or TiO_2 Merck POM supported samples. The results demonstrate that the Keggin type POM completely and partially degraded when supported on ZnO and Al_2O_3, respectively, and these binary solids always resulted as inactive for both catalytic and catalytic photo-assisted reactions.

The presence of UV light improved the activity of almost all POM supported materials. Also in this case, the interaction between POM and the support played a fundamental role for the photo-assisted catalytic reaction. Indeed, a stronger interaction, related also with the acidity of the POM supported samples could give rise to a POM excitation at lower energy irradiation. Moreover, an electron transfer from the conduction band of the semiconductor supports (TiO_2 or WO_3) to the excited POM to form the heteropolyblue species must also be considered.

Acknowledgements

The authors wish to thank MIUR (Rome) and Università degli Studi di Palermo for financial support. C'nano – Ile de France is acknowledged for financial support with the TRMC setup.

References

1 G. Ertl, H. Knözinger and J. Weitkamp, *Handbook of Heterogeneous Catalysis*, Wiley Vch Verlag Gmbh, Weinheim, 2008.
2 M. P. Atkins, *US Patent* 5 616 815, 1997.
3 G. J. Haining, *US Patent* 5 714 429, 1998.
4 I. V. Kozhevnikov, *Catalysis for Fine Chemical Synthesis. Vol. 2: Catalysis by Polyoxometalates*, John Wiley and Sons, Chichester, 2002.
5 V. Kozhevnikov, *Chem. Rev.*, 1998, **98**, 171.
6 A. V. Ivanov, E. Zausa, Y. Ben Taarit and N. Essayem, *Appl. Catal., A*, 2003, **256**, 225.
7 A. Hiskia, A. Mylonas and E. Papaconstantinou, *Chem. Soc. Rev.*, 2001, **30**, 62.
8 R. C. Chambers and C. L. Hill, *Inorg. Chem.*, 1991, **30**, 2776.

9 A. Fujishima, T. N. Rao and D. A. Tryk, *J. Photochem. Photobiol., C*, 2000, **1**, 1.
10 A. L. Linsebigler, G. Lu and J. T. Yates, *Chem. Rev.*, 1995, **95**, 735.
11 A. Di Paola, G. Marcì, E. García-López and L. Palmisano, *J. Hazard. Mater.*, 2012, **211–212**, 3.
12 V. Balzani, F. Bolleta, M. T. Gandolfi and M. Maestri, *Top. Curr. Chem.*, 1978, **75**, 1.
13 E. Papacostantinou, *Chem. Soc. Rev.*, 1989, **18**, 1.
14 H. Park and W. Choi, *J. Phys. Chem. B*, 2003, **107**, 3885.
15 Y. Yang, Y. Guo, C. Hu, Y. Wang and E. Wang, *Appl. Catal., A*, 2004, **273**, 201.
16 G. Marcì, E. García-López, L. Palmisano, D. Carriazo, C. Martin and V. Rives, *Appl. Catal., B*, 2009, **90**, 497.
17 G. Marcì, E. García-López and L. Palmisano, *Catal. Today*, 2009, **144**, 42.
18 F. Ma, T. Shi, J. Gao, L. Chen, W. Guo, Y. Guo and S. Wang, *Colloids Surf., A*, 2012, **401**, 166.
19 R. N. Biboum, C. P. N. Njiki, G. Zhang, U. Kortz, P. Mialane, A. Dolbecq, I. M. Mbomekalle, L. Nadjo and B. Keita, *J. Mater. Chem.*, 2012, **21**, 645.
20 R. Sivakumar, J. Thomas and M. Yoon, *J. Photochem. Photobiol., C*, 2012, **13**, 277.
21 J. M. Herrmann, *Catal. Today*, 1999, **53**, 115.
22 N. Mizuno and M. Misono, *Chem. Rev.*, 1998, **98**, 171.
23 L. R. Pizzio, C. V. Cáceres and M. N. Blanco, *Appl. Catal., A*, 1998, **167**, 283.
24 P. Vazquez, L. Pizzio, G. Romanelli, J. Autino, C. Caceres and M. Blanco, *Appl. Catal., A*, 2002, **235**, 233.
25 I. V. Kozhevnikov, A. Sinnema, R. J. J. Jansen, K. Pamin and H. van Bekkum, *Catal. Lett.*, 1994, **30**, 241.
26 F. Marme, G. Coudurier and J. C. Vedrine, *Microporous Mesoporous Mater.*, 1998, **22**, 151.
27 W. Kim, M. Kim, J. Kim and G. Seo, *Microporous Mesoporous Mater.*, 2003, **57**, 113.
28 A. Bielanski, A. Lubanska, J. Pozniczek and A. Micek-Ilnicka, *Appl. Catal., A*, 2003, **238**, 239.
29 L. R. Pizzio, P. G. Vazquez, C. V. Caceres and M. N. Blanco, *Appl. Catal., A*, 2003, **256**, 125.
30 J. G. Hernandez-Cortez, T. López, M. E. Manriquez, R. Gómez and J. Navarrete, *J. Sol–Gel Sci. Technol.*, 2003, **26**, 213.
31 B. Bachiller-Baeza and J. A. Anderson, *J. Catal.*, 2002, **212**, 231.
32 S. Jiang, Y. Guo, C. Wang, X. Qu and L. Li, *J. Colloid Interface Sci.*, 2007, **308**, 208.
33 S. R. Mukai, T. Sugiyama and H. Tamon, *Appl. Catal., A*, 2003, **256**, 99.
34 S. Hodjati, K. Vaezzadeh, C. Petit, V. Pitchon and A. Kiennemann, *Top. Catal.*, 2001, **16–17**, 151.
35 G. Marcì, E. García-López and L. Palmisano, *Appl. Catal., A*, 2012, **421–422**, 70.
36 X. Chen, L. Liu, P. Y. Yu and S. S. Mao, *Science*, 2011, **331**, 746.
37 S. J. Gregg and K. S. Sing, *Adsorption, Surface Area and Porosity*, Academic Press, San Diego, 2nd edn, 1982.
38 M. D. Ward, J. R. White and A. J. Bard, *J. Am. Chem. Soc.*, 1983, **105**, 27.
39 J. R. White and A. J. Bard, *J. Phys. Chem.*, 1985, **89**, 1947.
40 A. M. Roy, G. C. De, N. Sasmal and S. S. Bhattacharyya, *Int. J. Hydrogen Energy*, 1995, **20**, 627.
41 W. Macyk, G. Burgeth and H. Kisch, *Photochem. Photobiol. Sci.*, 2003, **2**, 322.
42 M. Kunst and G. Beck, *J. Appl. Phys.*, 1986, **60**, 3558.
43 C. Colbeau-Justin, M. Kunst and D. Huguenin, *J. Mater. Sci.*, 2003, **38**, 2429.
44 C. A. Emilio, M. I. Litter, M. Kunst, M. Bouchard and C. Colbeau-Justin, *Langmuir*, 2006, **22**, 3606.
45 D. Raoufi, *Renewable Energy*, 2013, **50**, 932.
46 J. Li, W. Kang, X. Yang, X. Yu, L. Xu, Y. Guo, H. Fang and S. Zhang, *Desalination*, 2010, **255**, 107.
47 A. Molinari, A. Bratovcic, G. Magliacca and A. Maldotti, *Dalton Trans.*, 2010, **39**, 7826.
48 A. Molinari, R. Amadelli, A. Mazzacani, G. Sartori and A. Maldotti, *Langmuir*, 2002, **18**, 5400.
49 A. Maldotti, A. Molinari, G. Varani, M. Lenarda, L. Storaro, F. Bigi, R. Maggi, A. Mazzacani and G. Sartori, *J. Catal.*, 2002, **209**, 210.
50 A. Micek-Ilnicka, *J. Mol. Catal. A: Chem.*, 2009, **308**, 1.
51 F. P. Koffyberg, K. Dwight and A. Wold, *Solid State Commun.*, 1979, **30**, 433.
52 Y. I. Kim, S. J. Atherton, E. S. Brigham and T. E. Mallouk, *J. Phys. Chem.*, 1993, **97**, 11802.
53 Y. Yang, Q. Wu, Y. Guo, C. Hu and E. Wang, *J. Mol. Catal. A: Chem.*, 2005, **225**, 203.
54 C. Wang, Q. Li, B. Mao, E. Wang and C. Tian, *Mater. Lett.*, 2008, **62**, 1339.
55 D. Carriazo, M. Del Arco, E. García-López, G. Marcì, C. Martín, L. Palmisano and V. Rives, *J. Mol. Catal. A: Chem.*, 2011, **342–343**, 83.
56 S. K. Sampath and J. F. Cordaro, *J. Am. Ceram. Soc.*, 1998, **81**, 649.
57 M. T. Pope, *Heteropoly- and isopolyoxometalates*, Springer-Verlag, New York, 1983.
58 C. Rocchiccioli-Deltcheff, M. Fournier, R. Franck and R. Thouvenot, *Inorg. Chem.*, 1983, **22**, 207.
59 J. Navarrete, T. López, R. Gómez and F. Figueras, *Langmuir*, 1996, **12**, 4385.
60 U. Lavrenčič Štangar, N. Grošelj and P. h. Colomban, *Chem. Mater.*, 2000, **12**, 3745; G. A. Parks, *Chem. Rev.*, 1965, **65**, 177.
61 P. Madhusudhan Rao, A. Wolfson, S. Kababya, S. Vega and M. V. Landau, *J. Catal.*, 2005, **232**, 210.
62 G. A. Parks, *Chem. Rev.*, 1965, **65**, 177.
63 I. Dosuna-Rodriguez, C. Adriany and E. M. Gaigneaux, *Catal. Today*, 2011, **167**, 56.

